Stress investigation on a cracked craze interacting with a nearby circular inclusion in polymer composites

Zhang, Yan Mei; Zhang, W. G.; Fan, M.; Xiao, Zhong Min

2016

Zhang, Y. M., Zhang, W. G., Fan, M., & Xiao, Z. M. (2017). Stress investigation on a cracked craze interacting with a nearby circular inclusion in polymer composites. Acta Mechanica, 228(4), 1213-1228.

https://hdl.handle.net/10356/83165

https://doi.org/10.1007/s00707-016-1773-4

Stress investigation on a cracked craze interacting with a near-by circular inclusion in polymer composites

Y. M. Zhang[1], W. G. Zhang[2], M. Fan[3] and Z. M. Xiao[1,*]

1. School of Mechanical and Aerospace Engineering
Nanyang Technological University, Singapore 639798
2. School of Civil Engineering, Chongqing University, Chongqing, China 400045
3. State Key Laboratory of Mechanics and Control of Mechanical Structures,
College of Aerospace Engineering,
Nanjing University of Aeronautics & Astronautics, Nanjing, China 210016

[*]Tel.: (65) 6790 4726 Fax: (65) 67911859 Email: mzxiao@ntu.edu.sg

Abstract

In polymer composites, inclusions (fillers) are introduced into the glassy polymeric matrixes in order to improve the toughness properties as the brittleness is one of the fatal drawbacks for glassy polymers. The first time in our current study, the stress analysis has been performed on the interaction between a circular inclusion and a craze with an internal small crack in polymeric composites. A craze can be treated as a crack with fibrils bridging the two crack surfaces. The forces applied by the fibrils to the crack surfaces (pulling the two surfaces closer) depend on the crack opening displacement. However, the crack opening displacement is directly related on the forces applied by the craze fibrils. To solve this dilemma, an iterative procedure is proposed for the first time to solve the formulated singular integral equations. The craze thickness profiles, the cohesive stress distribution and the fracture toughness of the polymeric composites are investigated thoroughly. Moreover, due to the influence of the inclusion, the uneven craze thickness profiles are observed from the left to the right part of the entire craze zone.

Keywords: Craze; Crack; Stress intensity factor; Fracture Mechanics; Composites; Glassy polymers.

1. Introduction

Recently a lot of research efforts have been put to develop polymer-based composites to satisfy the ever-increasing industry demand to accommodate a green and sustainable society [1]. This demand requires such materials with the multifunction and high performance, as single-phased polymeric materials cannot meet these requirements. Hence, carbon blocks, clays and carbon nano-fillers are added into the polymeric matrix in order to improve the mechanical, electrical and thermal properties of polymeric composite.

The fillers as the inclusions in the polymer matrices are tailored over a wide range of length scaled from nano-meters to micro meters. The past couple decades have witnessed a burst of experimental studies in the nature and entanglement of the polymers with the inclusions, especially in improving the toughness of polymeric composites. For instance, the application of the single-wall carbon nanotube was observed to improve the interfacial interaction and reduce the composite brittleness [2]. Sub-micron inclusions can substantially increase the fracture toughness in epoxy composites [3]. Reinforcing the glass, silica and alumina fillers sized up to 300 um into epoxy composites showed that the weakly bonded fillers would enhance the fracture properties. The toughness of epoxy composites was increased at higher volume fraction [4-6]. Meanwhile, in the microscopic view, the effects of particle size and volume fraction on the nanocomposite structure under deformation were studied by Monte Carlo dynamic simulations [7]. The toughness of the composites made of glassy polymer and nanotube fillers was increased significantly by a high inclusion density (2.0 wt%) [8].

It is generally recognized that the crazing is common in polymers. Nevertheless, in all the studies reviewed above, little research work has been found on the interaction between the craze and the inclusions in polymeric composites. A thin band of porous material termed as a

craze was observed in a glassy polymer from Kambour's experiments [9-11]. Crazing is considered as the first stage of the fracture process under steady loading in polymers. Crazes initiate, develop and grow into cracks which may lead to the failure through fracture of polymers. Therefore, to understand the interaction between the craze and the inclusion on the toughness properties of polymeric composites is indeed desirable in engineering practice.

From the mechanical aspect, a craze is treated as a crack fully or partially bridged by fibrils. For the stress distribution on the craze, one of the first attempts done by Knight [12], was to determine the displacement and stress distributions through the Fourier transform method, under the assumption of the craze with a uniform thickness. Later Lauterwasser and Kramer [13] obtained the craze thickness profile experimentally, based on the electron microscope observation, in order to determine the stress distributions along the craze. In this point, several methods were adopted for analytical and numerical investigations on the craze thickness profiles and stress distribution, such as the distributed dislocation method [14] and the superposition of Green's functions [15]. Nonlinear relationship between the stress and the craze thickness was considered to examine the growth of craze [16]. A simple model of craze tip stress amplification induced by cross-tie fibrils was proposed to estimate the failure of polymers [17]. In addition, Paris law model was adopted for the analysis of the craze growth problem in the glassy polymers [18].

All the above mentioned research works were concerned with the craze in a single homogeneous polymer material. With the increasing application of polymer composites, when a craze is initiated in a polymer composite, the interaction between the craze and the inclusion (the filler phase) will greatly influence the composite's fracture toughness and failure behavior.

In our current study, the influences of a near-by circular inclusion on the craze behaviors and the fracture toughness of the glassy polymers are investigated for the first time. The craze zone with a central small crack is considered since it is one of the common crazing cases in polymeric composites. The distributed dislocation method is employed to analyze the cohesive stress distributions along a craze interacting with different sized inclusions. Using the edge dislocation density as the Green's function, the physical problem of the interaction between a circular inclusion and a craze with an internal small crack in the glassy polymers is formulated into a set of singular integral equations, as given in Section 2. An iterative procedure is proposed to solve the craze thickness profiles, combined with the singular integral equations in this section as well. Results and discussion are given in Section 3. Validations on the numerical procedure with the empirical results are carried out. A series of the parametric studies are conducted to investigate the influences of the inclusion's elastic properties and their geometrical configurations on the craze behaviors. Major and significant conclusions arrived at in this study are summarized in the last Section.

2. Methodology

2.1. Problem formulation

Consider an infinite elastic polymer matrix which contains a circular inclusion with different mechanical properties. A craze with an internal small crack near the circular inclusion in the polymeric composite is illustrated in Fig. 1. The craze is assumed to be oriented along the radial direction of the circular inclusion. A uniform tensile stress is applied on the polymeric composite in the far field. For the craze, the cohesive stress distribution exerted by the fibrils on the craze region is represented by $P(x)$. Here what we have done is that we imaginarily cut off all the fibrils partly connecting the top and bottom surfaces of the craze, and add the

cohesive force from the fibrils to the surfaces. So the craze is equivalent to a crack with distributed cohesive stress $P(x)$ applied on part of the top and bottom surfaces.

Fig. 1

For the polymeric composite material, the matrix (termed as phase 1 labelled by "1" in Fig. 1) occupies the region of $r > r_0$, while the circular inclusion (termed as phase 2 labelled by "2" in Fig. 1) occupies the region of $r \le r_0$. The polymer matrix has the shear modulus μ_1 and Poisson's ratio ν_1 as its elastic properties. Similarly, the shear modulus μ_2 and Poisson's ratio ν_2 represent the inclusion's elastic properties. The craze is of length *2c*, and the internal small crack is of length *2a*. With respect to the proximity, the distance from the center of the inclusion to the left craze tip is denoted by t_1. It should be noted that $t_1 = L + r_0$.

2.1.1. Loading and boundary conditions

The loading and boundary conditions for the craze-inclusion problem in polymers are prescribed as follows. For polymer matrix, the far field loading is given by a uniform tensile stress:

$$\sigma_{yy}^{\infty} = \sigma_{\infty},\ \sigma_{xy}^{\infty} = 0. \tag{1}$$

The resulting stress from the far field loading at the craze surfaces is expressed as [19,20],

$$T_y(x,0) = \sigma_{\infty}[1 + \frac{\mu_1}{2(\lambda_1 + \mu_1)}(\frac{r_0}{x})^2 a_2 - \frac{3}{2}(\frac{r_0}{x})^2 b_3]. \tag{2}$$

Where the coefficients a_2 and b_3 can be obtained through

$$a_2 = -\frac{\mu_2 - \mu_1 + \lambda_2 - \lambda_1}{\lambda_2 + \mu_1 + \mu_2}, b_3 = \frac{\mu_2 - \mu_1}{\mu_2 \kappa_1 + \mu_1}.$$

Here $\kappa_1 = 3-4\nu_1$ for the plane strain condition and $\kappa_1 = (3-\nu_1)/(1+\nu_1)$ for the plane stress analysis. λ is one of the Lame's parameters, given by $\lambda = 2\mu\cdot\nu/(1-2\nu)$.

For the craze surfaces, the cohesive stress exerted by the fibrils is given by

$$D_y(x) = -P(x) \text{ for } t_1 \le x \le t_1 + (c-a) \,\&\, t_1 + (c+a) \le x \le t_1 + 2c \,. \tag{3}$$

Therefore, at the craze surfaces, the total stresses can be expressed as

$$\sigma_{yy}(x) = \begin{cases} T_y(x) - P(x), & for \quad t_1 \le x \le t_1 + (c-a) \quad , \quad t_1 + (c+a) \le x \le t_1 + 2c \\ T_y(x) \quad , & for \quad t_1 + (c-a) < x < t_1 + (c+a) \end{cases}. \tag{4}$$

2.1.2. Formulation of the current physical problem

To formulate the current physical problem of the craze-inclusion interaction, the craze is treated as a pile-up of dislocations based on the distributed dislocation method. Since in this study the uniaxial tensile loading as Mode I loading is considered, only the climbing dislocation density $B_y(\mathrm{x})$ for the edge dislocation is adopted to represent the craze. The spatial relationship between a single dislocation and the circular inclusion is presented in Fig. 2. The entire craze is taken to be located on the *x*-axis since it lies along the radial direction of the circular inclusion. Using the single edge dislocation solution as the Green function [21,22], the traction at the point (*x*, 0) due to the dislocation density along the craze zone is given by

$$\sigma_{yy}(x,0) = -\frac{2\mu_1}{\pi(\kappa_1+1)}\left[\int_{t1}^{t2} \frac{B_y(\xi)}{\xi - x} d\xi + \int_{t1}^{t2} k_1(\mathrm{x},\xi) B_y(\xi) d\xi\right]. \tag{5}$$

Where $t_2 = t_1 + 2c$.

Fig. 2

Substituting Eq. (4) into Eq.(5) leads,

$$\frac{1}{\pi}[\int_{t1}^{t2}\frac{B_y(\xi)}{\xi-x}d\xi+\int_{t1}^{t2}k_1(\mathrm{x},\xi)B_y(\xi)d\xi]=\frac{\kappa_1+1}{2\mu_1}\sigma_{yy}(\mathrm{x}). \tag{6}$$

Meanwhile, based on the distributed dislocation method, the dislocation densities for the whole craze must satisfy:

$$\int_{t1}^{t2}B_y(\xi)d\xi=0. \tag{7}$$

In Eq. (6), $k_1(\mathrm{x},\xi)$ is the relevant influence function, expressed as follows [22],

$$\begin{aligned}k_1(\mathrm{x},\xi)=&\frac{x_2}{r_2^2}[\frac{2Ax_2^2}{r_2^2}-\frac{B+5A}{2}]-\frac{x}{r^2}[\frac{2Ax^2}{r^2}-\frac{B+5A}{2}]\\&+\frac{2Ax_2L}{r_2^4d^2}[\frac{4x_2^2}{r_2^2}(\mathrm{L}-x_2)+((5-d^2)x_2-\frac{3L}{2})]\\&-\frac{r_0[\mathrm{A}(2d^2-1)+\mathrm{Q}-1]}{2r^2d}-\frac{AL}{r_2^2}(\frac{2}{d^2}-1)\\&+\frac{r_0x}{r^4}[r_0A(\frac{4x^2}{r^2}-3)+\frac{x}{d}(\mathrm{A}(2d^2-1)+\mathrm{Q}-1)]\end{aligned}. \tag{8}$$

Where

$r=\sqrt{x^2+y^2}$, $r_2=\sqrt{x_2{}^2+y^2}$, $x_1=x-\xi$, $x_2=x_1+L$, $L=r_0(\mathrm{d}^2-1)/\mathrm{d}$, $d=\xi/r_0$.

The elastic constants are:

$$A=\frac{\beta-\alpha}{1+\beta},\ B=-\frac{\beta+\alpha}{1-\beta},\ Q=\frac{(1+\alpha)(1-\alpha)}{(1-\beta)(1+\alpha-2\beta)}.$$

Here α, β are the Dundurs' parameters, given by

$$\alpha=\frac{\mu_2(\kappa_1+1)-\mu_1(\kappa_2+1)}{\mu_2(\kappa_1+1)+\mu_1(\kappa_2+1)},\ \beta=\frac{\mu_2(\kappa_1-1)-\mu_1(\kappa_2-1)}{\mu_2(\kappa_1+1)+\mu_1(\kappa_2+1)}.$$

2.1.3. Cohesive stress

In past literature, for simplicity, it is assumed that the constant cohesive stress is applied throughout the craze zone, similar with the crack problems in the small scale yielding zone [23]. Based on certain experimental observations, recent studies attempted to link the cohesive stress distribution profile $P(x)$ with the vertical displacement $v(x)$ of the craze. For instance, Ungsuwarungsri & Knauss employed several *P-v* relationships to obtain the craze initiation and craze growth problems [16,15]. In order to explore the influence of the *P-v* relationship on the craze-inclusion interaction problems, three different types of the *P-v* relationship are considered. If the craze thickness profile, i.e., the vertical displacement $v(x)$ is known, the cohesive stress $P(x)$ can be obtained by

$$P(x) = m \cdot E' \cdot v(x), \tag{9a}$$

$$P(x) = m \cdot E' \cdot (v(x))^{1.1}, \tag{9b}$$

$$P(x) = m \cdot E' \cdot (v(x))^{0.9}. \tag{9c}$$

Where $E' = E$ for plane stress and $E' = E/(1-\nu^2)$ for plane strain, m is the coefficient, $m=0.25$ is adopted in this study based on experimental observations [16,15]. Given the plane strain conditions, the curves of *P(x)* versus *v(x)* for the three different types are plotted in Fig. 3.

Fig. 3

2.2. Numerical procedure

As the physical problem of craze-inclusion interaction is formulated into a series of singular integral equations, the next step is to solve these equations (Eq. (6) and Eq. (7)), and subsequently to obtain the dislocation density $B_y(x)$. Once $B_y(x)$ is obtained, the vertical displacement profile of the craze can be calculated accordingly. Moreover, other significant

parameters, such as the cohesive stress distribution and the stress intensity factors at both craze tips, can also be derived.

Since the craze is considered as a crack partially bridged by the fibrils in polymers, the singularity at the both craze tips are the inverse square root of *x*, the same as the crack problems. Thus, the dislocation density should have $-1/2$ singular item on both craze tips. With this in mind, we let

$$B_y(x) = w(x)F_y(x)\,. \tag{10}$$

Where $F_y(x)$ is bounded functions in $t_1 \le x \le t_2$, and $w(x) = (x - t_1)^{-1/2}(t_2 - x)^{-1/2}$.

To simplify the integral domain, the new two variables, *s* and *t* are introduced to shift the interval of the integral throughout the whole craze zone from (t_1, t_2) to $(-1,1)$. They are written as

$$x = \frac{t_2 - t_1}{2}t + \frac{t_2 + t_1}{2},$$

$$\xi = \frac{t_2 - t_1}{2}s + \frac{t_2 + t_1}{2}\,. \tag{11}$$

Then, Eqs. (6) and (7) are rewritten in terms of *s* and *t* as:

$$\frac{1}{\pi}\left[\int_{-1}^{1}\frac{B_y(s)}{s-t}ds + \int_{-1}^{1}k_{11}(t,s)B_y(s)ds\right] = \frac{\kappa_1 + 1}{2\mu_1}\sigma_{yy}(t)\,, \tag{12}$$

$$\int_{-1}^{1}B_y(s)ds = 0\,. \tag{13}$$

Where

$$k_{11}(t,s) = \frac{t_2 - t_1}{2}k_1\left(\frac{t_2 - t_1}{2}t + \frac{t_2 + t_1}{2}, \frac{t_2 - t_1}{2}s + \frac{t_2 + t_1}{2}\right).$$

2.2.1. Discretization

The discretization method is employed to solve Eq. (12) and (13) numerically. Based on the numerical method developed by Erdogan and Gupta[24], the singular integral equation Eq. (12) can be discretized into (*n-1)* linear algebraic equations, expressed as below

$$\sum_{k=1}^{n}\frac{1}{n}F_y(\mathrm{s}_k)[\frac{1}{\mathrm{s}_k-u_r}+\mathrm{k}_{11}(u_r,\mathrm{s}_k)]=\frac{\kappa_1+1}{2\mu_1}\sigma_{yy}(x_r)\,. \tag{14}$$

Where *n* is the number of discretized terms used, and

$$\mathrm{s}_k=\cos(\frac{\pi(2\,\mathrm{k}-1)}{2n}),\mathrm{k}=1,...,\mathrm{n}\,,$$

$$u_r=\cos(\frac{\pi r}{n}),\text{where}\,r=1,...,\mathrm{n}-1\,,\text{and}\;x_r=\frac{t_2-t_1}{2}\mathrm{u}_r+\frac{t_2+t_1}{2}\,.$$

Similarly, Eq. (13) is discretized into the following linear algebraic equation,

$$\sum_{k=1}^{n}\frac{1}{n}F_y(\mathrm{s}_k)=0\,. \tag{15}$$

In summary, Eq. (14) and Eq. (15) provide a system of *n* linear algebraic equations to determine the *n* unknown parameter $F_y(\mathrm{s}_1),...,F_y(\mathrm{s}_n)$. In this study, the discretized number *n*=500 is the best compromise between the convergence accuracy (within 0.1%) and the computational time.

2.2.2. Iterative procedure

In the formulated equations, the cohesive stress $P(x)$ is a function of the vertical displacement $v(x)$ (as given in Eq. (9)), while the vertical displacement $v(x)$ is a function of the dislocation density $B_y(x)$. But to solve the dislocation density $B_y(x)$ from the *n* linear algebraic equations mention above, we need to know how much the cohesive stress $P(x)$ is. To solve this dilemma, an iterative solution procedure is specially designed to solve the cohesive stress $P(x)$ at the craze zone.

Step 1: we assume an initial form of the vertical displacement $v^0(x)$ as

$$v^0(x) = \sqrt{v_{\max}{}^2 \cdot (1-(\mathrm{x}-\mathrm{t}_1-c)^2 / c^2)} \,. \tag{16}$$

Where $v_{\max}$ is presumed as the maximum value of the vertical displacement. It is found that a properly selected $v_{\max}$ will make the iterative convergence fast. Here *c* is the half craze length.

Step 2: based on the initial assumed $v^0(x)$, the initial cohesive stress $P^0(x)$ is calculated by Eq. (9) only for the craze region indicated by Eq. (3). Then it is substituted into Eq. (4).

Step 3: as the total stresses on the craze surfaces given by Eq. (4) are evaluated, the first-round iterative results for $F_y(\mathrm{s}_1),...,F_y(\mathrm{s}_n)$ are determined through solving an array of Eqs (14, 15). Once the variable $F_y(\mathrm{s}_k)$ is obtained, the dislocation density $B_y(x)$ can be evaluated by Eq. (10).

Step 4: based on the distributed dislocation method, the vertical displacement of the craze can be obtained by

$$v^i(x) = \int_{t_1}^{x} B(\xi) d\xi \,. \tag{17}$$

A new iteration procedure will restart again with the new vertical displacement $v^i(x)$ evaluated from the above equation. For the iteration procedure, the convergence is achieved when it satisfies $(v^i(x) - v^{i-1}(x)) / v^{i-1}(x) \le 0.1\%$.

Lastly, with the numerical solutions of the dislocation density, the Mode I stress intensity factors on the left and right craze tips [25] are given as below

$$K_I^L = -\lim_{\xi \to t_1} \frac{2\mu_1 \sqrt{2\pi(\xi - \mathrm{t}_1)}}{\kappa_1 + 1} B_y(\xi) = \frac{-2\mu_1 \sqrt{\pi(\mathrm{t}_2 - \mathrm{t}_1)/2}}{\kappa_1 + 1} F_y(-1), \tag{18a}$$

$$K_I^R = \lim_{\xi \to t_2} \frac{2\mu_1 \sqrt{2\pi(\mathrm{t}_2 - \xi)}}{\kappa_1 + 1} B_y(\xi) = \frac{2\mu_1 \sqrt{\pi(\mathrm{t}_2 - \mathrm{t}_1)/2}}{\kappa_1 + 1} F_y(+1). \tag{18b}$$

Where, the superscripts L and R represent the left and right craze tips, respectively.

3. Results and Discussion

In this section, the influence of a circular inclusion on the fracture behaviors of the craze with an internal small crack in the glassy polymers is investigated thoroughly. The stress intensity factor, as one of the significant fracture parameters, is adopted to represent the toughness behaviors of the polymeric composite for various inclusion's material properties and different craze-inclusion geometrical configurations. Moreover, the craze thickness profile and the cohesive stress exerted by the fibrils are evaluated under the assumption of several *P-v* relationships. It should be noted that all the numerical examples considered are assumed to be in the plane strain state.

3.1. Comparison of the stress intensity factors with the empirical results

As presented in the previous section, the numerical procedure to solve the craze-inclusion physical problem is tedious, particularly in the expressions of the singular integrals and those discretized equations. As a result, mistakes or slight errors may be introduced during compiling the program codes. To avoid possible errors, the solution of the stress intensity factor for the craze problem given by Tada et al. [26] is used to verify the analytical results obtained from the current work. To perform the validation on our analytical results, the circular inclusion is assumed to have the same material properties with the polymeric matrix. So the current problem is reduced to a craze in a homogeneous polymer without the inclusion, which is the case studied by Tada et al. [26].

The stress intensity factor K_I for the craze problem in an infinite 2-D case under the far field tensile loading, is given by the following equation,

$$K_I = S\sqrt{\pi c} - 2S_{br}\sqrt{c/\pi}\arccos(a/c). \tag{19}$$

Where *S* represents the far field tensile loading, *c* is the half craze length, *a* is the half length of the internal small crack and S_{br} is the average value of the cohesive stress on the craze surfaces.

The values of the stress intensity factors obtained from our current work and Eq. (19) are listed in Table 1, for different far field loadings, craze lengths and internal crack lengths. It can be observed that the relative errors are less than 1% for all the cases considered. The negligible relative errors indicate that the results obtained from the current work are in good agreement with the solution of K_I from Tada's book. In other words, the numerical procedure to solve the craze-inclusion problem presented in this study is reliable and accurate.

Table 1

3.2.Craze thickness profile

There are many factors affecting the fracture behaviors of the craze, such as the matrix and the inclusion's material properties, the distance between the craze and inclusion, and the loadings. Since the primary concern in this study is the craze-inclusion interaction and the corresponding fracture behaviors of the polymeric composites, the far field loading is assumed to be constant as $\sigma_\infty = 33.0MPa$. Also, the numerical examples considered in the following sections are calculated with the following parameters: $\mu_1 = 2.0GPa$, $\nu_1 = \nu_2 = 0.33$, $c = 100\mu m$. For a better understanding of crazing phenomenon in polymer composites, we

concentrate on the following parameters: the variations of relative shear modulus ratio μ_2 / μ_1, the relative inclusion size r_0 / c, the ratio *a/c* and the relative crack-inclusion distance L / c. Those parameters are used to carry out the investigation on the fracture behaviors of the crazed polymeric composites.

The craze thickness profiles for three different ratios of *a/c* are plotted in Fig. 4, under the condition that $r_0 / c = 2.0$, $L / c = 0.5$, $\mu_2 / \mu_1 = 10$, and the *P-v* type 1 are considered. In the figure, u_r is a dimensionless variable and its value (-1.0 ~ 1.0) represents the whole craze region (including the internal crack). It can be observed that at $u_r = 0.0$ (i.e., at the center of the internal crack), the case of $a / c = 0.5$ has the maximum value of crack thickness. While the case of $a / c = 0.1$ produces the minimum value of crack thickness (which is around $1.1 \mu m$). The possible reason for this observation is that in the case of $a / c = 0.1$, the longer cohesive zone is involved, and subsequently, the larger cohesive forces exerted by the fibrils are applied on the craze surfaces. It leads to the smaller crack opening displacement. Moreover, the uneven craze thickness profiles for the three curves are observed between the left and right part throughout the craze zone. The right craze zone has relatively larger craze thickness values than those at the left craze zone. For instance, in the case of $a / c = 0.5$ the value of craze thickness is $0.6 \mu m$ at $u_r = -0.8$, while it is around $0.8 \mu m$ at the symmetry point $u_r = 0.8$. Clearly it is due to the effect of the near-by circular inclusion. Here $\mu_2 / \mu_1 = 10$ is considered, it means that the inclusion has a harder stiffness, compared to the polymeric matrix. Consequently, the harder inclusion has the more shielding effect on the left craze zone, which will produce smaller value of craze thickness.

Fig. 4

Next is to examine the influence of the *P-v* relationships, the craze thickness profiles for the three different *P-v* types are plotted in Fig. 5, in which the parameters are considered as follows: $a_0 / c = 0.2$, $r_0 / c = 2.0$, $L / c = 0.5$ and $\mu_2 / \mu_1 = 10$. It is found that as a whole, the shapes of the craze thickness profiles are similar for the three *P-v* types. However, at a given location of the craze zone, the largest value of craze thickness is obtained by using the *P-v* type 2. On the contrary, it produces the smallest value of craze thickness under the *P-v* type 3.

Fig. 5

3.3.Cohesive stress distribution

With the parameters of $r_0 / c = 2.0$, $L / c = 0.5$ and $\mu_2 / \mu_1 = 10$, Fig. 6 shows the cohesive stress distributions along the craze zone for three different internal crack sizes. Here the *P-v* type 1 is assumed. It is obvious that the uneven cohesive stress profiles between the left and right craze zone are observed due to the stiffer inclusion ($\mu_2 / \mu_1 = 10$) considered. Another observation is that at the right craze zone $u_r > 0$, the cohesive stress ahead of the internal crack tip increases gently with the increasing ratio *a/c*.

Fig. 6

Meanwhile, the cohesive stress distributions along the craze zone for the three different *P-v* types are shown in Fig. 7. It can be observed that the maximum value of the cohesive stress is obtained ahead of the internal crack tip for all the cases. Additionally, at any value of u_r, the maximum cohesive stress is obtained from the case of the *P-v* type 3. Whereas, the case of the *P-v* type 2 has the smallest cohesive stress.

Fig. 7

3.4. Fracture behaviors of the craze

In this study the stress intensity factors at the left and right craze tips are normalized by the results from the homogeneous crack case (without the inclusion) for better understanding the inclusion's influence on the craze. They are expressed by $nK_I^L = K_I^L / (\sigma_\infty \sqrt{\pi c})$ and $nK_I^R = K_I^R / (\sigma_\infty \sqrt{\pi c})$, respectively.

3.4.1. Influence of shear modulus ratio

For condition $a/c = 0.1$, $L/c = 0.5$ and *P-v* type 1, the curves of nK_I^L and nK_I^R against the shear modulus ratios of the inclusion/matrix are plotted in Fig. 8 for various inclusion sizes. In this figure, the solid straight line represents the normalized stress intensity factor obtained from the homogenous craze case (i.e., $\mu_2 / \mu_1 = 1$).

When the shear modulus ratio μ_2 / μ_1 is greater than 1, both nK_I^L and nK_I^R values are below the solid straight line, and both decrease with the increasing shear modulus ratio. That means, the shielding effect of the inclusion on the craze is observed due to the stiffer inclusion (i.e., $\mu_2 / \mu_1 > 1$). In general, the stiffer the inclusion is, the higher the shielding effect is achieved. As a result, it leads to smaller stress intensity factor as shown in the figure. The normalized stress intensity factors nK_I^L and nK_I^R versus the shear modulus ratios become stabilized when μ_2 / μ_1 is greater than 15, where the inclusion becomes much stiffer than the matrix and is nearly rigid.

When the shear modulus ratio μ_2 / μ_1 is less than 1, both the normalized stress intensity factors nK_I^L and nK_I^R values are above the solid straight line, and they decreases significantly

as the value of μ_2 / μ_1 increases up to 1.0. Here $\mu_2 / \mu_1 < 1$ means that the inclusion has a "softer" stiffness compared to the polymeric matrix. Under this situation, the anti-shielding effect of the softer inclusion on the craze is observed. As shown in Fig. 8(a) the value of nK_I^L reaches 2.3 for the case of $r_0 / c = 10$, indicating that the large softer inclusion plays a significant anti-shielding effect on the fracture behavior of the near-by craze.

Another interesting observation is that for the case of $r_0 / c = 0.5$, the curve of nK_I^R against the shear modulus ratio is much closer to the straight line than that of nK_I^L at any shear modulus ratio. It reveals that compared to the left craze zone, the right craze zone is less affected by the relatively small inclusion even if the inclusion is a stiffer material.

Fig. 8

3.4.2. Influence of P-ν types

Considering the case $\mu_2 / \mu_1 \geq 1$, the normalized stress intensity factor variations of nK_I^L and nK_I^R with the shear modulus ratio μ_2 / μ_1 are presented in Fig. 9 for the three different *P-ν* relationships. Here $a / c = 0.2$, $r_0 / c = 2.0$ and $L / c = 1.0$ are considered. The first observation is that the values of nK_I^L and nK_I^R decreases with the increasing ratio μ_2 / μ_1. In Fig. 9(a) it is observed that given any value of μ_2 / μ_1, the maximum value of nK_I^L is obtained from the case of *P-ν* type 2, while the case of *P-ν* type 3 has the minimum value of nK_I^L. The similar trend is found in Fig. 9(b) for the value of nK_I^R. This observation indicates that the *P-ν* type 3 which produces the smaller stress intensity factors, can enhance the shielding effect of a stiffer inclusion on the craze. While the *P-ν* type 2 can decrease the shielding effect of a

stiffer inclusion. In this study, the *P-v* type 1 as a moderate solution is considered for the following parametric studies.

Fig. 9

3.4.3. Influence of a/c

To investigate the effect of the internal crack size on the fracture behaviors of the entire craze, we take the following ratios $r_0 / c = 2.0$, $L / c = 0.5$ and *P-v* type 1. The variations of nK_I^L and nK_I^R with the ratio *a/c* are shown in Fig. 10 for the three different shear modulus ratios. The value of nK_I^L as shown in Fig. 10(a) increases with the increasing ratio *a/c*. It suggests that for any shear modulus ratio considered, the internal crack becomes larger, and it will result in a larger stress intensity factor. Moreover, it is observed that the value of nK_I^L obtained from the case of $\mu_2 / \mu_1 = 0.1$ are much greater than the other two cases, due to the anti-shielding effect of the softer inclusion on the craze. In Fig. 10(b) the curves of nK_I^R versus the ratio *a/c* show the similar trend as those in Fig. 10(a). Another interesting observation is that for the case of $\mu_2 / \mu_1 = 10$, the very gentle slopes are observed for both curves of nK_I^L and nK_I^R, indicating that the effect of the ratio *a/c* on the fracture behaviors of the craze can be negligible for the case when a stiffer inclusion is considered.

Fig. 10

3.4.4. Influence of L/c

In order to examine the influence of craze-inclusion distance on fracture behaviors of the polymeric composites, the curves of nK_I against the variable *L/c* for two different inclusion sizes are plotted in Fig. 11. Here $a / c = 0.2$ is considered. For $\mu_2 / \mu_1 = 10$ shown in Fig.

11(a), it is observed that both nK_I^L and nK_I^R are less than 0.78 (which is the value obtained from the homogenous case) due to the shielding effect of the stiffer inclusion on the craze. When *L/c* is less than 1.0, the value of nK_I^L is considerably smaller than that of nK_I^R. This is because the left craze tip is close to the stiff inclusion, and its fracture behavior is dominated by the significant shielding effect of the stiff inclusion. However, for a small inclusion with $r_0 / c = 0.5$, the values of nK_I^L and nK_I^R are almost the same when L / c is greater than 3.0. For the large inclusion with $r_0 / c = 10.0$, both nK_I^L and nK_I^R are approaching to each other when L / c is greater than 15.0. As the distance increases, the shielding effect of the inclusion is getting weaker and weaker, so the fracture behaviors of the two craze tips are beyond the influencing zone of the inclusion. When the inclusion is further away from the craze, the normalized stress intensity factors is close to 0.78 (especially for the small inclusion). It indicates that the interaction of the inclusion and craze could be neglected at such a large craze-inclusion distance, and the craze can be treated as in pure polymeric matrix.

Similarly, the normalized stress intensity factors with the values greater than 0.78 are found in Fig. 11(b) for $\mu_2 / \mu_1 = 0.1$. The values of nK_I^L and nK_I^R decrease with the increasing *L/c* value. Particularly, the two curves of nK_I^L against the ratio L / c are of exponential decreasing trend as the ratio L / c increases. For instance, at $L / c = 0.5$, the value of nK_I^L obtained from the case of $r_0 / c = 10.0$ can reach up to 2.0, due to the significant anti-shielding effect by the larger and softer inclusion.

In summary, Fig. 11 demonstrates that a short craze-inclusion distance has significant influence on the fracture behaviors of the craze. Given the shear modulus ratio and the inclusion size, the short craze-inclusion distance can largely magnify the shielding effect of

the stiffer inclusion. On the other hand, it can also prompt the anti-shielding effect of the softer inclusion on the craze.

Fig. 11

4. Conclusions

The first time in our current study, the analytical solution for the interaction between a craze (with an internal small crack) and a near-by circular inclusion in glassy polymer is presented. An iterative procedure is proposed to solve the formulated singular integral equations. The detailed numerical procedure is given to obtain the stress intensity factors at the both craze tips. Based on systematic parametric studies, the craze thickness profiles, the cohesive stress distribution and the fracture toughness of the polymeric composites are investigated. The main conclusions are summarized as below:

1) Comparisons of the stress intensity factors obtained from the current work and the empirical equation in open literature demonstrate that the solution procedure on the craze-inclusion interaction problem presented in this study is reliable and accurate.
2) The uneven craze thickness profiles are observed between the left and right part throughout the craze zone due to the near-by inclusion considered. A stiffer inclusion has stronger shielding effect on the left craze zone (which is nearer to the inclusion), and results in smaller craze thickness.
3) When the shear modulus ratio $\mu_2 / \mu_1 > 1$, both the normalized stress intensity factor nK_I^L and nK_I^R values decrease with the increasing shear modulus ratio, due to the shielding effect of a stiffer inclusion on the craze. This shielding effect reaches a plateau when $\mu_2 / \mu_1 > 15$. While for $\mu_2 / \mu_1 < 1$, anti-shielding effect is observed. The normalized stress intensity factors increase exponentially with the decreasing shear modulus ratio.

4) When the central crack inside the craze zone is larger, it results in a larger stress intensity factor of the craze.

In our following work, a craze interacting with many surrounding inclusions in glassy polymer composites will be investigated. Moreover, due to the softening, the internal crack propagation will be taken into account once the craze thickness reaches a certain value. Meanwhile, complicated loading conditions such as biaxial loadings will be considered in our future work.

References

1. Utracki, L.A., Jamieson, A.M.: POLYMER PHYSICS from suspensions to nanocomposites and beyond. Wiley, Hoboken, New Jersey (2010)
2. Tonpheng, B., Yu, J., Andersson, B.M., Andersson, O.: Tensile strength and young's modulus of polyisoprene/single-wall carbon nanotube composites increased by high pressure cross-linking. Macromolecules **43**(18), 7680-7688 (2010). doi:10.1021/ma101484e
3. He, R., Zhan, X., Zhang, Q., Zhang, G., Chen, F.: Control of inclusion size and toughness by reactivity of multiblock copolymer in epoxy composites. Polymer (United Kingdom) **92**, 222-230 (2016). doi:10.1016/j.polymer.2016.04.003
4. Kitey, R., Tippur, H.V.: Role of particle size and filler-matrix adhesion on dynamic fracture of glass-filled epoxy. I. Macromeasurements. Acta Materialia **53**(4), 1153-1165 (2005). doi:10.1016/j.actamat.2004.11.012
5. Kitey, R., Tippur, H.V.: Role of particle size and filler-matrix adhesion on dynamic fracture of glass-filled epoxy. II. Linkage between macro- and micro-measurements. Acta Materialia **53**(4), 1167-1178 (2005). doi:10.1016/j.actamat.2004.11.011
6. Moloney, A.C., Kausch, H.H., Stieger, H.R.: The fracture of particulate-filled epoxide resins - Part 1. J Mater Sci **18**(1), 208-216 (1983). doi:10.1007/BF00543827
7. Toepperwein, G.N., Karayiannis, N.C., Riggleman, R.A., Kröger, M., De Pablo, J.J.: Influence of nanorod inclusions on structure and primitive path network of polymer nanocomposites at equilibrium and under deformation. Macromolecules **44**(4), 1034-1045 (2011). doi:10.1021/ma102741r
8. Richardson, D.G., Abrams, C.F.: The effects of nanotube fillers on craze formation in simulated glassy polymers under tensile load. Molecular Simulation **33**(4-5), 421-427 (2007). doi:10.1080/08927020601154637

9. Kambour, R.P.: Structure and properties of crazes in polycarbonate and other glassy polymers. Polymer **5**(C), 143-155 (1964).

10. Kambour, R.P.: Mechanism of fracture in glassy polymers. III. Direct observation of the craze ahead of the propagating crack in poly(methyl methacrylate) and polystyrene. Journal of polymer science part B Polymer Physics **4**(3), 349-358 (1966).

11. Kambour, R.P.: Mechanism of fracture in glassy polymers. II. Survey of crazing response during crack propagation in several polymers. Journal of polymer science part B Polymer Physics **4**(1), 17-24 (1966).

12. Knight, A.C.: Stress crazing of transparent plastics. Computed stresses at a nonvoid craze mark. Journal of polymer science part A Polymer Chemistry **3**(5), 1845-1857 (1965).

13. Lauterwasser, B.D., Kramer, E.J.: Microscopic mechanisms and mechanics of craze growth and fracture. Philosophical Magazine A: Physics of Condensed Matter, Structure, Defects and Mechanical Properties **39**(4), 469-495 (1979). doi:10.1080/01418617908239285

14. Wang, W.C.V., Kramer, E.J.: A Distributed Dislocation Stress-Analysis for Crazes and Plastic Zones at Crack Tips. J Mater Sci **17**(7), 2013-2026 (1982). doi:Doi 10.1007/Bf00540419

15. Ungsuwarungsri, T., Knauss, W.G.: A Nonlinear Analysis of an Equilibrium craze: part I-Problem Formulation and Solution. Journal of Applied Mechanics, Transactions ASME **55**, 44-51 (1988).

16. Ungsuwarungsri, T., Knauss, W.G.: A Nonlinear Analysis of an Equilibrium craze: part II-simulations of craze and crack growth. Journal of Applied Mechanics, Transactions ASME **55**, 52-58 (1988).

17. Brown, H.R.: A molecular interpretation of the toughness of glassy polymers. Macromolecules **24**(10), 2752-2756 (1991).

18. Marissen, R.: Craze growth mechanics. Polymer **41**(3), 1119-1129 (2000). doi:10.1016/S0032-3861(99)00234-7

19. Hoh, H.J., Xiao, Z.M., Luo, J.: On the plastic zone size and crack tip opening displacement of a Dugdale crack interacting with a circular inclusion. Acta Mechanica **210**(3-4), 305-314 (2010). doi:10.1007/s00707-009-0211-2

20. Xiao, Z.M., Chen, B.J.: Stress intensity factor for a Griffith crack interacting with a coated inclusion. International Journal of Fracture **108**(3), 193-205 (2001). doi:10.1023/A:1011066521439

21. Xiao, Z.M., Chen, B.J.: Stress analysis for a Zener–Stroh crack interacting with a coated inclusion. International Journal of Solids and Structures **38**(28–29), 5007-5018 (2001). doi:http://dx.doi.org/10.1016/S0020-7683(00)00335-8

22. Hills, D.A.: Solution of Crack Problems: the Distributed Dislocation Technique. Dordrecht, Kluwer (1996)

23. Kramer, E.J., Hart, E.W.: Theory of slow, steady state crack growth in polymer glasses. Polymer **25**(11), 1667-1678 (1984). doi:10.1016/0032-3861(84)90164-2

24. Erdogan, F., Gupta, G.D.: Stresses near a flat inclusion in bonded dissimilar materials. International Journal of Solids and Structures **8**(4), 533-547 (1972). doi:10.1016/0020-7683(72)90021-2

25. Weertman, J.: Dislocation based Fracture Mechanics. World Scientific, Singapore (1996)

26. Tada, H., Paris, P.C., Irwin, G.R.: The stress analysis of cracks handbook. Del. Research Corporation, (1973)

Table Captions

Table 1 Values of the stress intensity factors obtained from current work and Eq. (19).

Table 1

σ_∞ **(*MPa*)**	c **(** μm **)**	a**(** μm **)**	K_I calculated by Eq.(19)	K_I obtained from current work	Relative error
20	100.00	10.00	8.6199	8.6382	0.21%
20	100.00	20.00	8.8184	8.8268	0.09%
33	100.00	10.00	14.2277	14.2577	0.21%
33	100.00	20.00	14.5517	14.5655	0.09%
45	100.00	10.00	19.3972	19.4381	0.21%
45	100.00	20.00	19.8380	19.8568	0.09%
33	50.00	5.00	10.0605	10.0818	0.21%
33	150.00	15.00	17.4253	17.4621	0.21%

Figure Captions

Fig. 1 Illustrative diagram of the craze-inclusion interaction problem: a craze with an internal small crack near a circular inclusion.

Fig. 2 The spatial relationship between a single edge dislocation and a circular inclusion.

Fig. 3 Curves of the three different *P-v* relationships considered in this study.

Fig. 4 Craze thickness profiles for the three different ratios of *a/c*.

Fig. 5 Craze thickness profiles for the three different *P-v* relationships.

Fig. 6 Cohesive stress distributions along the entire craze zone for three different ratios *a/c*.

Fig. 7 Cohesive stress distributions along the entire craze zone for the three different *P-v* relationships.

Fig. 8 (a) Curves of normalized stress intensity factor nK_I^L against the shear modulus ratios for various inclusion sizes. (b) Curves of normalized stress intensity factor nK_I^R against the shear modulus ratios for various inclusion sizes. The other parameters are considered as: $a/c = 0.1,\ L/c = 0.5$ and *P-v* type 1.

Fig. 9 (a) Curves of nK_I^L against the shear modulus ratio μ_2/μ_1 and (b) Curves of nK_I^R against the shear modulus ratio μ_2/μ_1 for three different *P-v* types, when $a/c = 0.2$, $r_0/c = 2.0$ and $L/c = 1.0$ are considered.

Fig. 10 (a) Curves of nK_I^L against the ratio *a/c* and (b) Curves of nK_I^R against the ratio *a/c* for three different shear modulus ratios when the following parameters $r_0/c = 2.0$, $L/c = 0.5$ and *P-v* type 1 are considered.

Fig. 11 Curves of nK_I against the ratio *L/c* for both craze tips: (a) for $\mu_2/\mu_1 = 10$ and (b) for $\mu_2/\mu_1 = 0.1$ when $a/c = 0.2$ and *P-v* type 1 are considered.

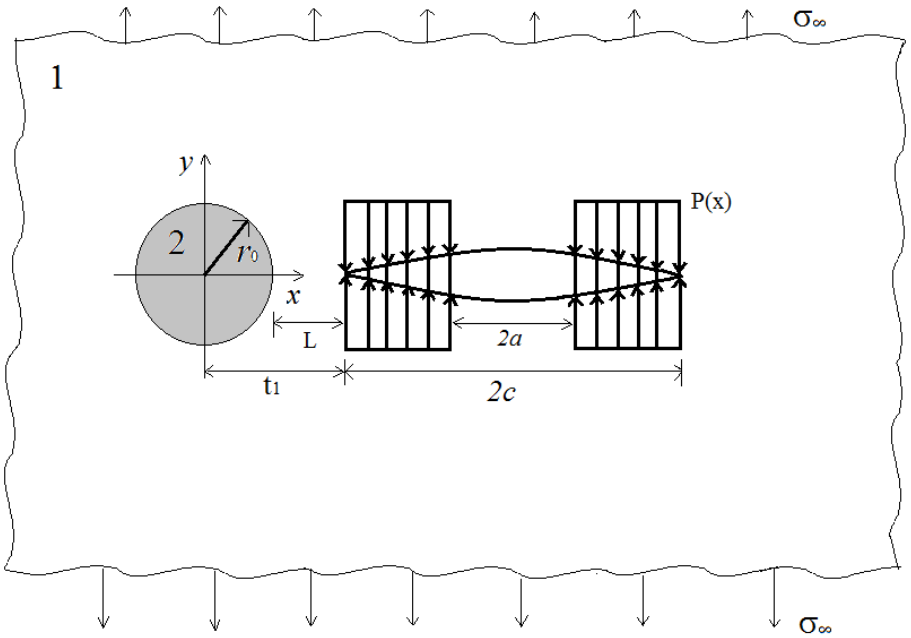

Fig. 1

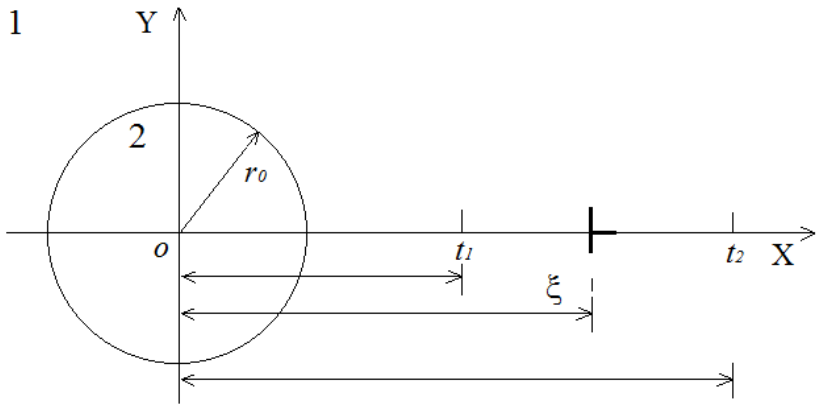

Fig. 2

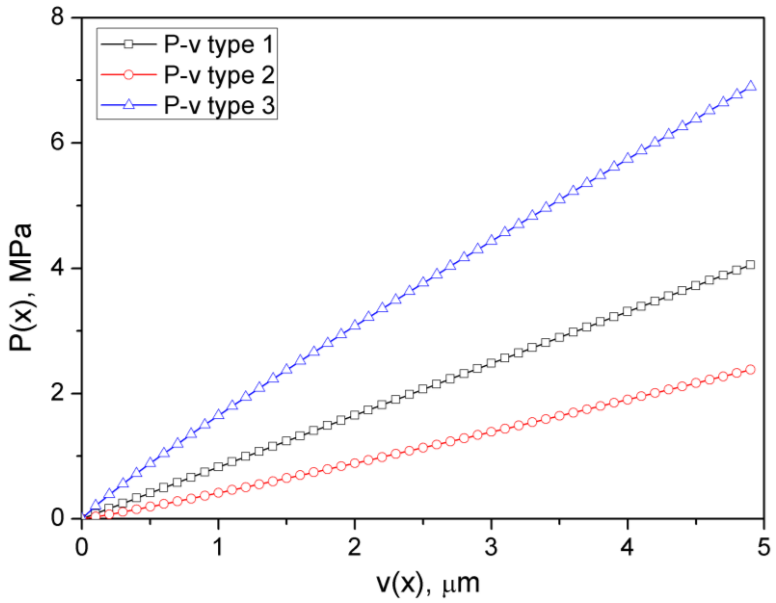

Fig. 3

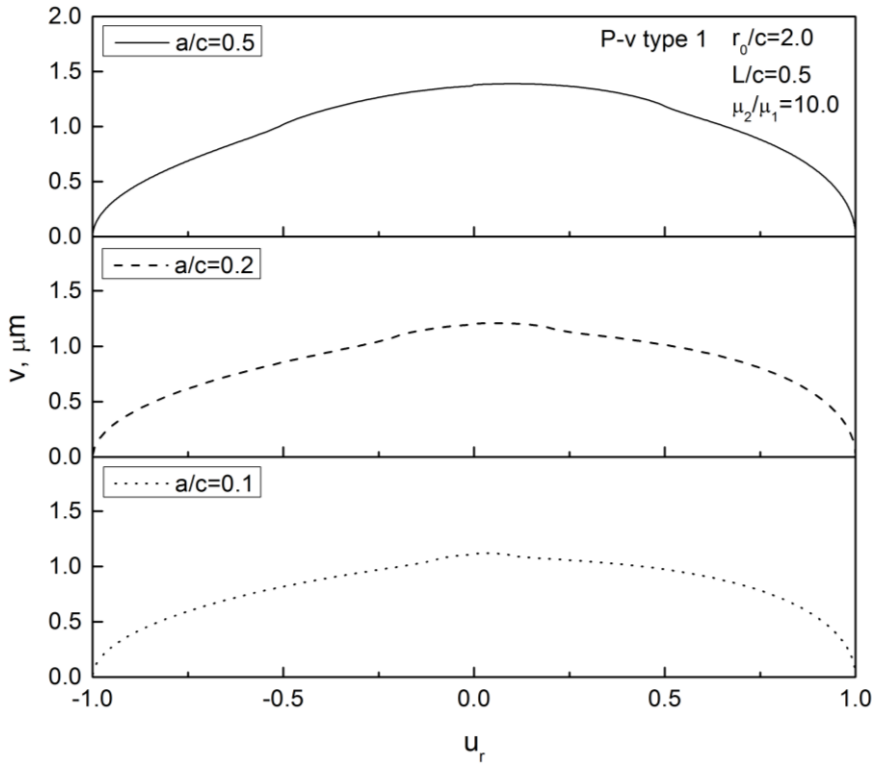
a/c=0.5
P-v type 1
r0/c=2.0
L/c=0.5
μ2/μ1=10.0
a/c=0.2
a/c=0.1
v, μm
ur

Fig. 4

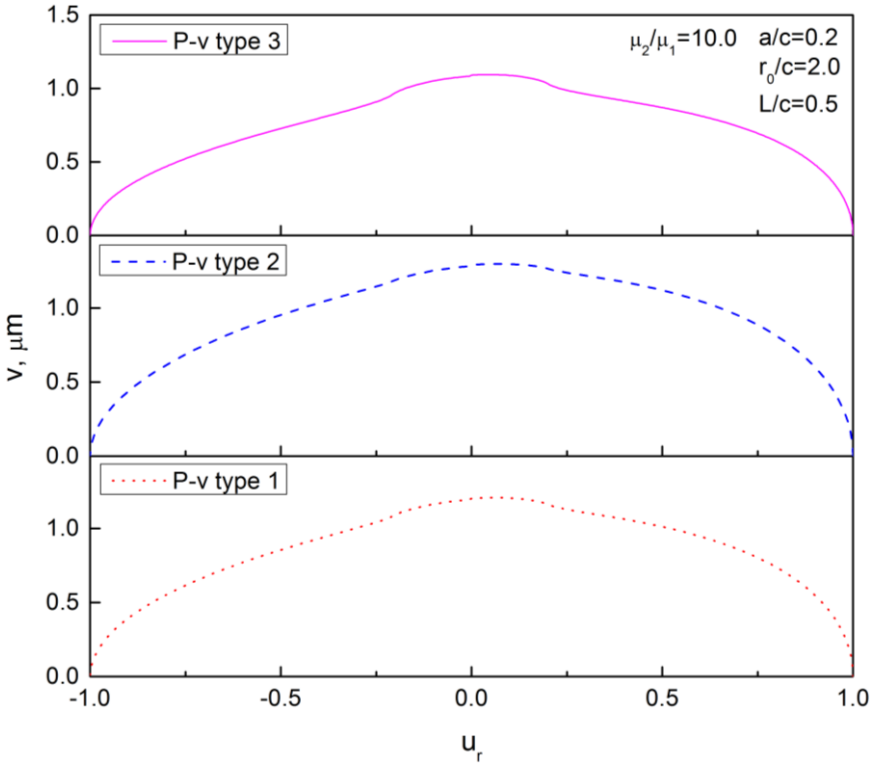
P-v type 3
μ2/μ1=10.0
a/c=0.2
r0/c=2.0
L/c=0.5
P-v type 2
P-v type 1
v, μm
ur

Fig. 5

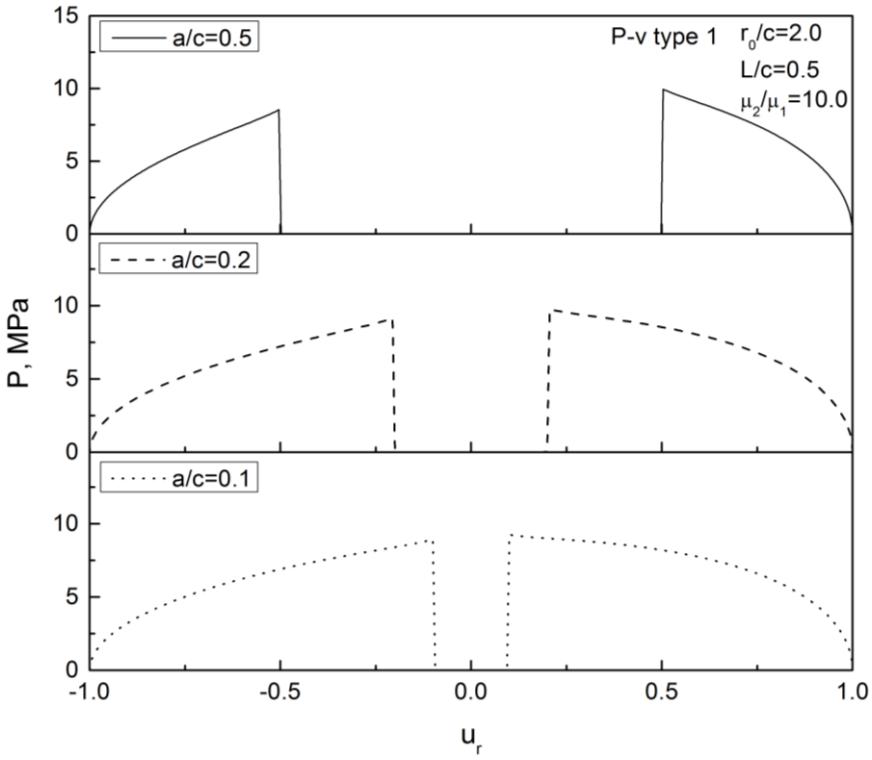
a/c=0.5
P-v type 1 r0/c=2.0
L/c=0.5
μ2/μ1=10.0
a/c=0.2
a/c=0.1
P, MPa
ur

Fig. 6

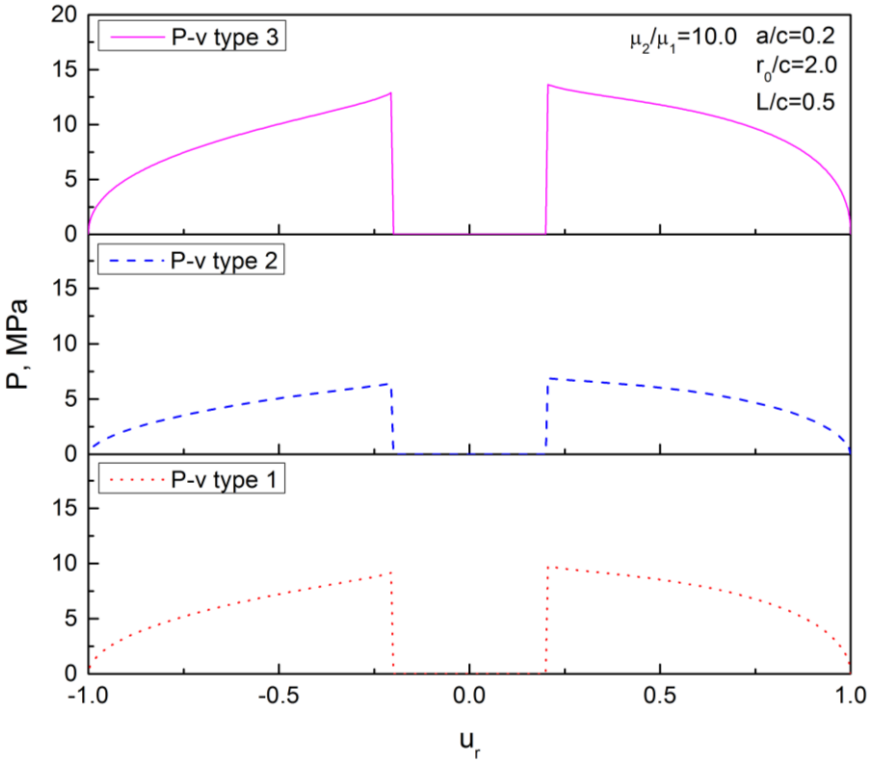
P-v type 3
μ2/μ1=10.0 a/c=0.2
r0/c=2.0
L/c=0.5
P-v type 2
P-v type 1
P, MPa
ur

Fig. 7

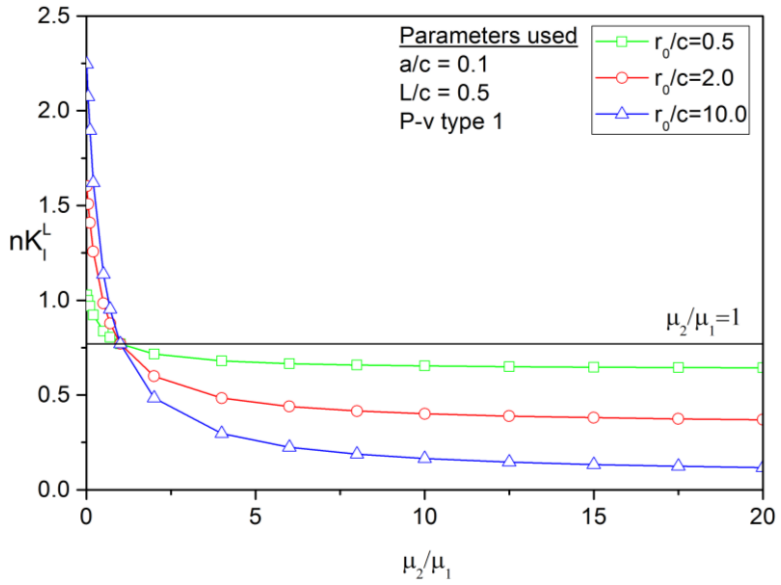
Parameters used
a/c = 0.1
L/c = 0.5
P-v type 1
r0/c=0.5
r0/c=2.0
r0/c=10.0
μ2/μ1=1
nK1L
μ2/μ1
0.0
0.5
1.0
1.5
2.0
2.5
0
5
10
15
20

(a)

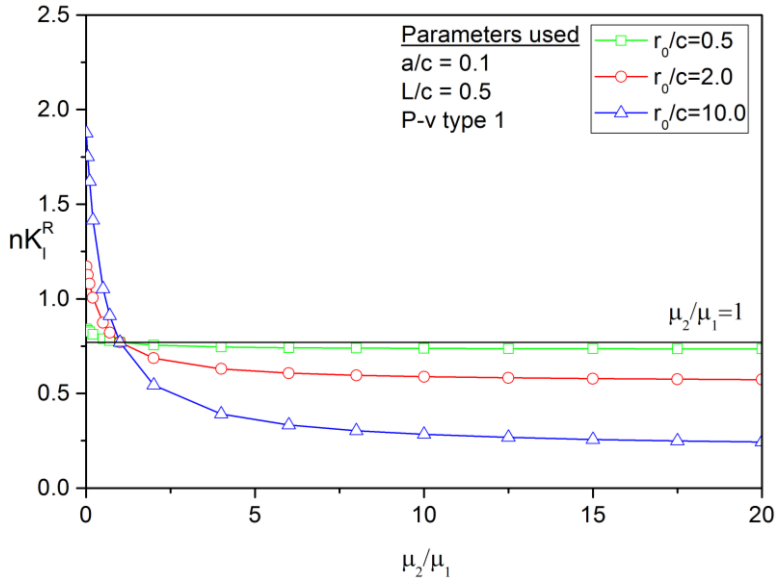
Parameters used
a/c = 0.1
L/c = 0.5
P-v type 1
r0/c=0.5
r0/c=2.0
r0/c=10.0
μ2/μ1=1
nK1R
μ2/μ1
0.0
0.5
1.0
1.5
2.0
2.5
0
5
10
15
20

(b)

Fig. 8

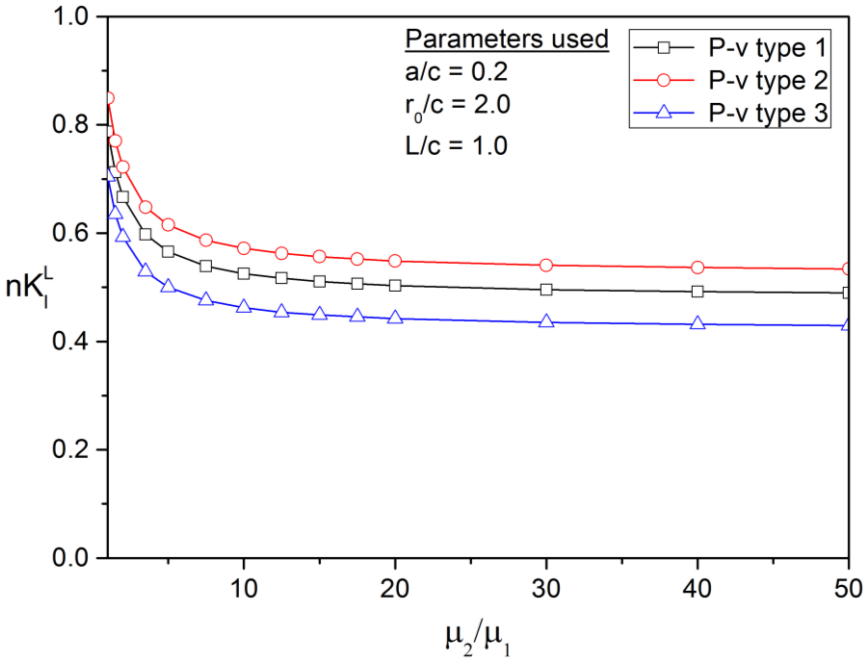
Parameters used
a/c = 0.2
r0/c = 2.0
L/c = 1.0
P-v type 1
P-v type 2
P-v type 3
nK_l^L
μ2/μ1
1.0
0.8
0.6
0.4
0.2
0.0
10
20
30
40
50

(a)

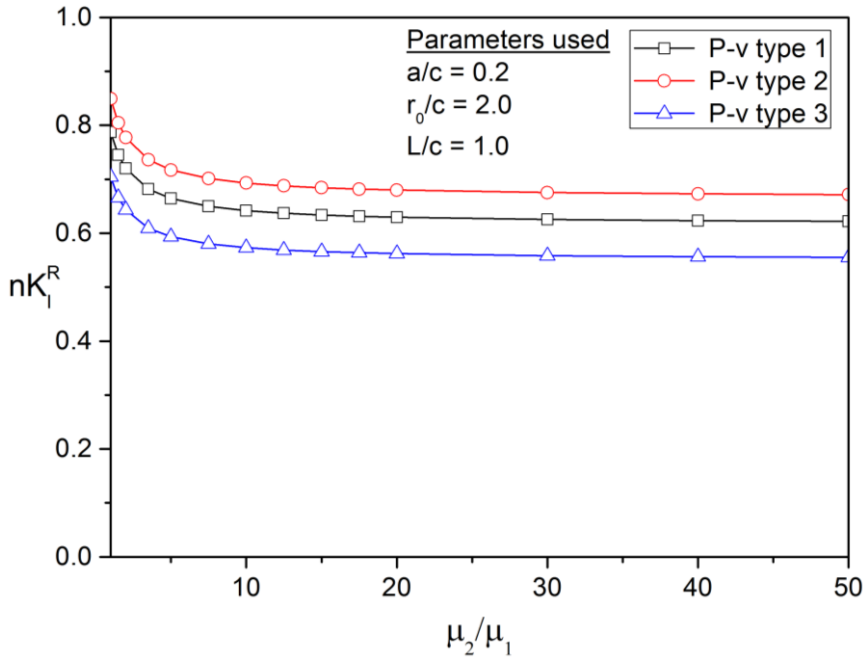
Parameters used
a/c = 0.2
r0/c = 2.0
L/c = 1.0
P-v type 1
P-v type 2
P-v type 3
nK_l^R
μ2/μ1
1.0
0.8
0.6
0.4
0.2
0.0
10
20
30
40
50

(b)

Fig. 9

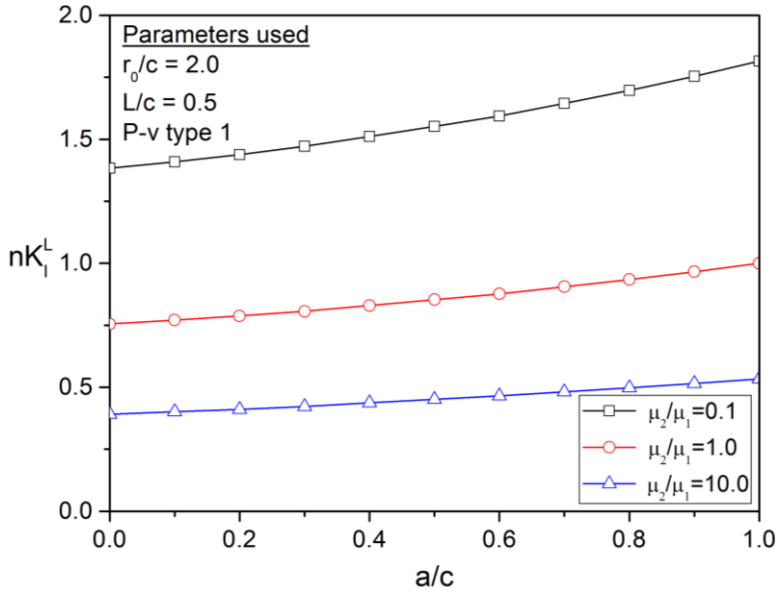
Parameters used
r0/c = 2.0
L/c = 0.5
P-v type 1
nK_I^L
a/c
μ2/μ1=0.1
μ2/μ1=1.0
μ2/μ1=10.0

(a)

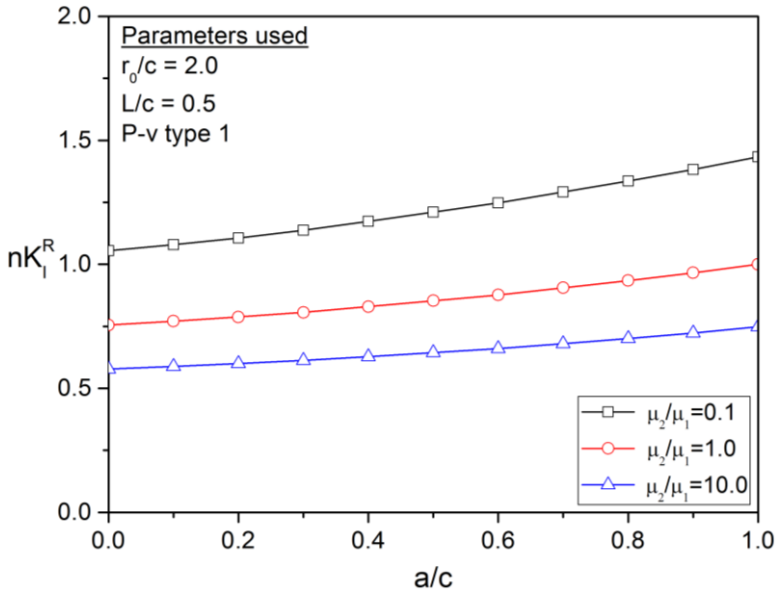
Parameters used
r0/c = 2.0
L/c = 0.5
P-v type 1
nK_I^R
a/c
μ2/μ1=0.1
μ2/μ1=1.0
μ2/μ1=10.0

(b)

Fig. 10

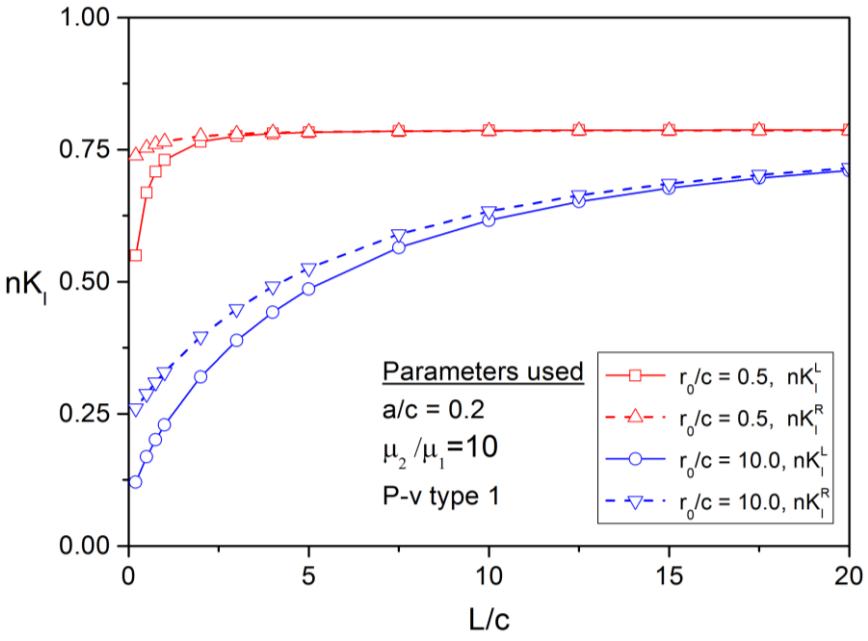
1.00
0.75
0.50
0.25
0.00
nK_I
0
5
10
15
20
L/c
Parameters used
a/c = 0.2
μ2 /μ1=10
P-v type 1
r0/c = 0.5, nK_I^L
r0/c = 0.5, nK_I^R
r0/c = 10.0, nK_I^L
r0/c = 10.0, nK_I^R

(a)

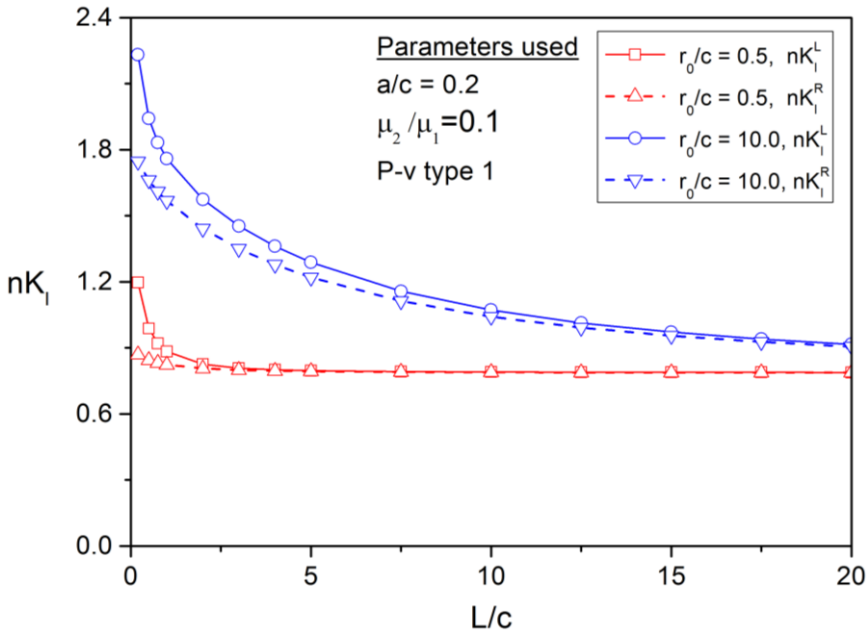
2.4
1.8
1.2
0.6
0.0
nK_I
0
5
10
15
20
L/c
Parameters used
a/c = 0.2
μ2 /μ1=0.1
P-v type 1
r0/c = 0.5, nK_I^L
r0/c = 0.5, nK_I^R
r0/c = 10.0, nK_I^L
r0/c = 10.0, nK_I^R

(b)

Fig. 11